Schottky and p-i-n Resonant Cavity Enhanced Photodiodes with High Handwidth-Efficiency products

G. Ulu [a], M. Gökkavas, M. S. Ünlü [b]
N. Bıyıklı, E. Özbay [c]
R. P. Mirin and K. A. Bertness and D. H. Christensen [d]

[a]Department of Physics,
[b] Department of Electrical and Computer Engineering, Boston University, Boston, MA 02215

[c]Department of Physics, Bilkent University, Ankara, Turkey, 06533.

[d]National Standards and Technology, Boulder, CO 80303.

1. INTRODUCTION

Optical communications has been the traditional driving force of the photodetector research. Local-area networks and short-distance communications have a growing demand for fast and efficient detectors to complement vertical-cavity surface-emitting lasers (VCSELs) in the 800-1000 nm range. VCSELs have emerged as the preferred sources owing to their tunability and high modulation-bandwidth.[1–3] Photodetectors with bandwidths up to 100 GHz and efficiencies up to 90 % have been demonstrated for this purpose in the 800-1000 nm wavelength range.[4,5] Beside communications, quantum optics also requires high-speed photodetectors with high quantum efficiencies (η). The outcomes of optical experiments that involve measurements of the fluctutations and correlations of light beams in quantum regime depend on the quantum efficiencies of the photodetectors. For example, the amount of quantum noise reduction observed with intensity-correlated twin beams[6,7] has been actually limited by, η. An "imperfect" detector mixes the vacuum modes with the signal modes at the point of detection. This phenomenon could also be considered as the introduction of a "partitioning noise". For η less than unity, the relation between the intrinsic quantum observables and the statistics of fluctuations become more complicated. Thus any realistic extraction of information from detection schemes such as a homodyne setup has to compensate for sub-unity η of the detectors.[8,9] In addition to perfect efficiency, fast temporal response is also called for, as pulsed sources are widely used in order to enhance interactions in the nonlinear media involved in these experiments. Typical source in the 800-1000 nm range are the mode-locked Ti:sapphire lasers which provide light pulses of a few picosecond wide at repetition rates at 80 MHz.

In this work, we describe theoretical and experimental studies of ultrafast resonant-cavity-enhanced (RCE) photodetectors with quantum efficiencies approaching unity for quantum optical applications.

2. DEVICE DESIGN AND FABRICATION

For a conventional detector,

$$\eta = (1 - R_{top})\,[1 - \exp(-\alpha d)] \tag{1}$$

where α is the absorption coefficient for an absorption layer of thickness d and R_{top} is the reflectance of the top surface. It is possible to build conventional detectors with very high η provided that R_{top} is eliminated by anti-reflection (AR) coating. However, the thick absorption regions would limit the high speed performance due to long transit times of the photogenerated carriers. Furthermore, thick active layers are hard to deplete and cause further limitation because of diffusion from the undepleted absorbing regions. On the other hand, high η values can be attained by RCE photodetection with relatively thin active layers due to the enhancement of the optical field in the active layer placed inside a Fabry-Perot cavity.[10] Figure X shows a comparison of conventional and RCE photodetectors in terms of dependence of peak η on the parameter αd. For a RCE detector with the GaAs-air interface as the top mirror, $\eta > 0.99$ can be achieved in a finite range of αd values around 0.65, corresponding to an absorption layer thickness an order of magnitude less than that for a conventional device with perfect AR coating.[10] In addition to reducing transit times, small

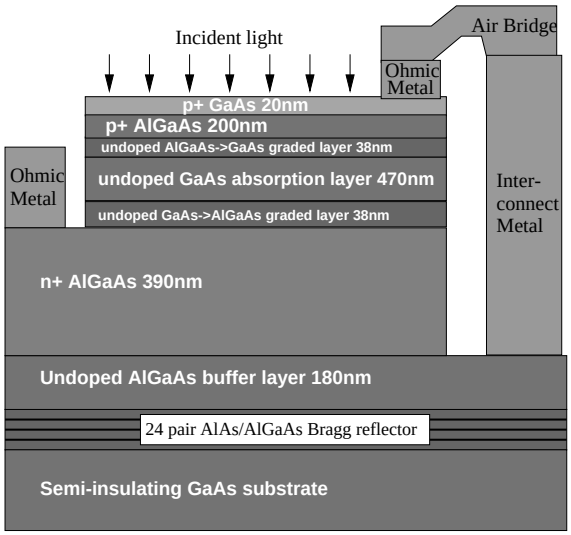

Figure 1. The cross-section of the device reveals the epilayer structure. Use of airbridges reduces parasitic capacitances.

absorption paths also eliminate secondary carrier recombination that could further limit η. The resonance can be adjusted by recessing the top surface of the device.

Figure 1 depicts the cross-section of the device. The epilayer structure was grown by solid-source molecular beam epitaxy on a semi-insulating GaAs substrate. An $Al_{0.2}Ga_{0.8}As$/GaAs p-i-n detector is placed in a low loss Fabry-Perot resonator formed by the semiconductor-air interface as the top mirror and a distributed Bragg reflector (DBR) as the bottom mirror. The DBR mirror consists of 24 quarter-wave stacks of $Al_{0.2}Ga_{0.8}As$/AlAs. Its stop band is designed for > 99 % reflectance in a 40 nm wavelength window centered around 820 nm. The active layer is 470 nm of intrinsic GaAs. The interfaces between the absorption layer and the doped regions are alloy-graded to avoid carrier trapping. The thickness is chosen according to the optimization: $R_{top} = R_{bottom} \exp(-2\alpha d)$.[10] We used scattering-matrix methods to calculate the reflectance and quantum efficiency of our designs. In Fig. X, we plot the measured and calculated reflectance of the structure as-grown. We also observed that the resonance wavelength shifts slightly to shorter wavelengths toward the edge of the wafer. According to our calculations, a $\sim 1\%$ thickness variation can account for this shift.

The devices were fabricated by a microwave-compatible process described elsewhere.[4] To optimize high-speed performance, we formed coplanar waveguides on the substrate. Airbridges made of 1 μm thick gold connect the center of the waveguides to the ohmic contacts of the device with minimal parasitic capacitance. The breakdown voltages of the photodiodes were over 14 V. The dark current in a device of 30 μm in diameter was 20 pA.

3. MEASUREMENTS

3.1. Quantum Efficiency

To characterize quantum efficiencies approaching unity, it is essential to collect all of the excitation on the device under test. We used a tunable continuous wave Ti:sapphire laser and single mode fibers for light delivery onto the detectors. In earlier measurements, we used a monochromated tungsten-halogen lamp coupled into a multimode fiber.[4] Those measurements were limited by poor spatial confinement in the core and light lost in cladding modes. In our setup, the low numerical aperture of the single-mode fiber yields a narrow circular beam, allowing for uniform illumination of small devices at normal incidence without bringing the fiber very close to the surface. For device sizes on the order of the optical mode in the fiber, a very small fiber-to-sample distance is required resulting in an optical cavity formation and causing an

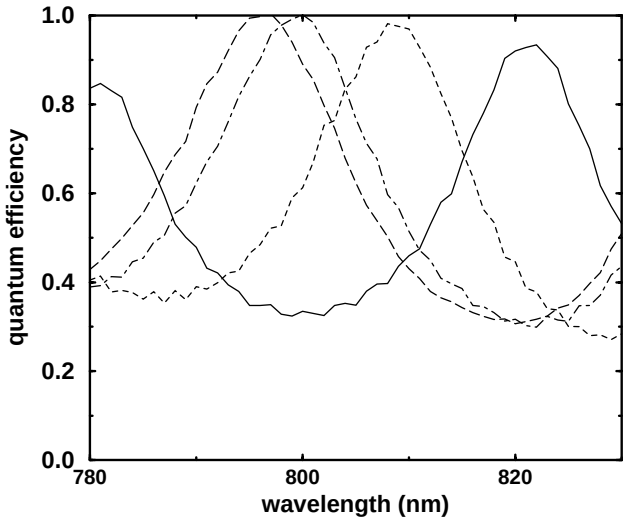

Figure 2. The resonance wavelength shifts toward shorter wavelengths as the top surface is recessed. The η of as-grown wafer is sub-unity, because the GaAs cap layer is not removed yet.

interference pattern. The output from the laser was split to provide a reference beam to track the laser power fluctuations.

In Fig. X, we plot the measured and calculated quantum efficiency of a 250 μm $\times$ 250 μm detector, that exhibits unity η at 800 nm. The accuracy of our measurements on large area devices was $\pm 2\%$ and was only limited by the responsivity data (supplied by the manufacturer) of the NIST-traceable detector used to calibrate the setup. We estimate two main sources of deviation from the design: one being the lack of reliable absorption data for GaAs, the other being the variations of layer thicknesses over the wafer during the growth, especially of the DBR mirror. In fact, the fit to the efficiency data in Figure X is made by assuming a 1% reduction in the thicknesses of the DBR layers. Figure 2 demonstrates the tunability of our devices after the fabrication by slow recess etches. The peaks preserve their finesse and efficiency along the tuning range determined by the stop band of the bottom mirror.

The results shown were recorded with no bias across the device. In fact, the spectral responses are not altered by application of reverse bias. This indicates that the entire active layer is already depleted by built-in field.

3.2. High-speed performance

We used a microwave probe station with a 50 GHz sampling oscilloscope and a mode-locked picosecond Ti:sapphire laser as the excitation. The smallest devices (14 μm $\times$ 8 μm) exhibited the fastest response governed by the transit time in the absorption region (Fig.3). The temporal response is 12 ps full-width-at half-maximum (FWHM). The measurement of these devices were limited by the speed of the sampling oscilloscope. When the response of the scope and excitation pulse width is subtracted, the estimated 3-dB bandwidth is more than 50 GHz.

For larger devices, the depletion capacitance is appreciable. We plot the normalized responses of several devices with varying sizes in Fig.4. The depletion capacitance is 0.25 fF/μm^2 corresponding to a f_{3dB-RC} of 10 GHz for a 40 μm $\times$ 40 μm device with R = 50 Ω.

As in efficiency measurements, the temporal responses were independent of the external bias and the results are shown for zero bias. We deduce that the intrinsic absorption regions were fully depleted with built-in voltage. Since the carriers are generated in the absorption region which is fully covered by the field, all of them are collected via drift process. Thus no diffusion process is involved in the response.

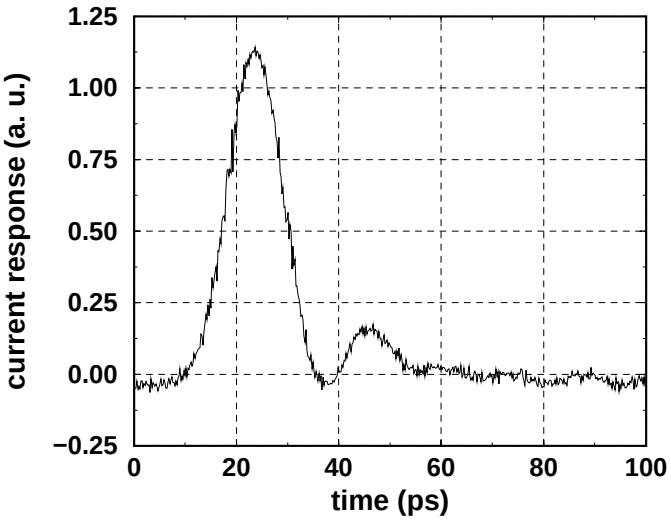

Figure 3. Temporal response of a device exhibiting $\tau_{\mathrm{FWHM}} = 12$ ps.

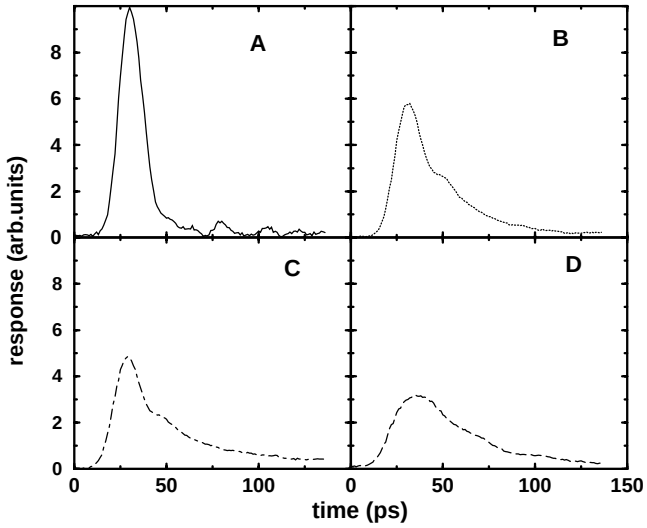

Figure 4. High speed responses from small and large devices. An RC tail evolves as the active area gets larger. A: 14 μm $\times$ 8 μm, and the diameters of the round detectors B, C, D are 30 μm, 60 μm, and 100 μm respectively.

We also observed in large devices that the sheet resistance of the top p^+ layer induces a finite risetime if the recess etch removes a significant portion of the doped layer. This effect is more pronounced as the beam size gets smaller compared to the device size. The thickness and the doping of this layer have to be chosen to make allowance for tuning etches without compromising the temporal response.

4. CONCLUSION

In conclusion, we designed, fabricated and characterized high-speed RCE photodetectors with near-unity quantum efficiency. The bandwidth-efficiency products of the detectors are in excess of 50 GHz. The resonance wavelengths were post-process adjustable in the spectral region 780-830 nm. The deviations from

the design were shown to be the result of approximately 1% error in crystal growth calibration. To the best of our knowledge, these devices are the fastest photodetectors with $\eta > 0.99$ measured to an accuracy of 2%. Picosecond temporal response combined with adjustable-wavelength near-unity η makes these RCE detectors suitable for quantum optical experiments especially those with pulsed lasers as well as for short-distance communication systems.

REFERENCES

1. A. K. Dutta, H. Kosaka, K. Kurihara, and Y. S. andK. Kasahara *IEEE J. Lightwave Technol.* **16**, pp. 870–875, 1998.
2. K. M. Hanson in *IEEE LEOS 1997 Annual Meeting*, LEOS, ed., *LEOS 97 Conference Proceedings* **2**, pp. 419–420, 1997.
3. P. Tayebati, P. Wang, D. Vakhshoori, C. Lu, M. Azimi, and R. N. Sacks *IEEE Photon. Techol. Lett.* **10**, pp. 1679–1681, 1998.
4. E. Özbay, N. Bıyıklı, I. Kimukin, O. Aytür, M. Gökkavas, G. Ulu, R. Mirin, D. Christensen, and M. S. Ünlü *Appl. Phys. Lett.* **to be published in 1999**.
5. B. M. Onat, M. Gokkavas, E. Ö. E. P. Ata, E. Towe, and M. S. Ünlü *IEEE Photonics Tech. Lett.* **10**, pp. 707–709, 1998.
6. P. Kumar and O. Aytür *Phys. Rev. Lett.* **64**, pp. 1015–1018, 1990.
7. O. Aytür and P. Kumar *Phys. Rev. Lett.* **65**, pp. 1551–1554, 1990.
8. K. Banaszek *Phys. Rev. A* **57**, pp. 5013–5015, 1998.
9. K. Banaszek and K. Wodkiewicz *Phys. Rev. A.* **55**, pp. 3117–3123, 1997.
10. M. S. Ünlü and S. Strite *J. Appl. Phys.* **78**, pp. 607–628, 1995.